Journal of Materials Chemistry A

PAPER

Electrochemical fabrication of transparent nickel hydroxide nanostructures with tunable superhydrophobicity/superhydrophilicity for 2D microchannels application†

Cite this: *J. Mater. Chem. A*, 2014, **2**, 1985

Ya-Huei Chang,[a] Yu-Ting Huang,[a] Man Kit Lo,[a] Chih-Fan Lin,[b] Chih-Ming Chen[b] and Shien-Ping Feng*[a]

Received 26th September 2013
Accepted 14th November 2013

DOI: 10.1039/c3ta13882h

www.rsc.org/MaterialsA

In order to survive in the harsh environments, natural creatures evolve unique wettability properties, for example, lotus leaf exhibits extreme water-repellency and Namib Desert beetle displays high wetting contrast patterns. Inspired by these natural creatures, a multifunctional surface which owns superhydrophobicity, widely tunable wettability (*i.e.* between superhydrophilic and superhydrophobic) and non-degraded transparency is developed. A facile and cost-effective approach *via* stepwise electrodeposition of nanosponge-like nickel hydroxide with the aid of self-assembled monolayers (SAMs) of non-fluorinated silane is introduced to well manipulate the pore size and surface energy. The exposed hydroxide ligands of nickel hydroxide films enhance water penetration and SAMs adsorption and thereby achieve tunable wettability from superhydrophilic to superhydrophobic. Meanwhile, the nanoscale roughness and sub-wavelength pore size of the films help maintain their optical transparency. The effectiveness of these achieved functions is demonstrated on the transparent 2D microfluidic channel fabricated by a simple electrochemical attach–detach patterning technique, which shows a fast flow speed of 5 mm s^{-1} because of the strong capillary force.

Introduction

Learning from nature with superhydrophilic/superhydrophobic properties, typically moss leaves and lotus leaves, inspires people to create various applications, such as self-cleaning, anti-icing, anti-fogging and anti-fouling.[1–4] Superhydrophilic surfaces are characterized by static water contact angles (WCAs) smaller than 10° whereas superhydrophobic surfaces are defined by WCAs larger than 150°. The external stimuli, such as UV light irradiation, electrical potential, and UVO_3 modification, can be used to achieve the superhydrophilic surface due to the increase of the surface energy.[5–7] Superhydrophobic surfaces can be fabricated by roughening the surface structures with "top-down" or "bottom-up" processes and modifying the surface chemical properties with low-surface-energy materials (fluorinated or hydrocarbon silanes, phosphates and thiols).[8–10] Other than superhydrophilic/superhydrophobic plants, a special Namib Desert beetle exhibits high wetting contrast to help it collect and uptake water to survive in the arid environment, which has boosted a great research interest in wettability manipulation techniques between superhydrophilic and superhydrophobic and emerging applications in micro-patterning, bio-chemical microsensors, cell encapsulations and microfluidic channels.[11,12]

If the wettability-tunable coatings can also be kept transparent, the range of applications will be extended to optical fields such as variable-focal-length microlenses, anti-reflection films of solar cells and in-planar bio-microfluidic channels.[13–17] However, the increase of the surface roughness when fabricating superhydrophobic surfaces makes maintainable transparency difficult due to the effect of Mie scattering. Furthermore, the fabrication methods must be simple and inexpensive. Therefore, a multifunctional coating possessing superhydrophobicity, widely tunable wettability and non-degraded transparency fabricated in a facile and cost-effective way is pivotal but challenging.

Some research groups have achieved optically transparent superhydrophobic surfaces, particularly on SiO_2-based materials, but the tunable wettability has seldom been investigated.[18–20] To broaden the applications, other research groups have developed a smart surface with the acceptably tunable

[a]*Department of Mechanical Engineering, The University of Hong Kong, Pokfulam Rd., Hong Kong, China. E-mail: hpfeng@hku.hk*

[b]*Department of Chemical Engineering, National Chung Hsing University, 250 Kuo Kuang Rd., Taichung, Taiwan, Republic of China*

† Electronic supplementary information (ESI) available: Supplementary text, Fig. S1–S6 (nucleation mechanism, AFM images, AC impedance, AFM images and comparison with theoretical wetting models) and Video S2–S3 (extreme water-repallancy and quick flow of microfluids in 2D microchannel). See DOI: 10.1039/c3ta13882h

wettability and optical transparency. Han *et al.* developed a wettability-tunable composite (125–155°) by mixing H_2O_2-treated thin multi-walled CNTs with fluorinated silane sol solution by varying the spraying amounts with a result of compromised transmittance (degraded from 95% to 65%). Although the transparency could be further improved by introducing the silica nanoparticles into the CNTs composite, the tunable wettability was lost.[21] Shen *et al.* synthesized ultra-thin In_2O_3 nanowires by a laser-ablation chemical vapour deposition method, which satisfied both the optical transparency (80%) and tunable wettability (from superhydrophilic to 143°) using UV illumination and controlling the wire diameters, but yet attained superhydrophobicity.[22] Up to now, very little research can use a simple and facile approach to fulfill these multifunctional requirements.

This paper therefore aims to electrochemically fabricate transparent nickel hydroxide ($Ni(OH)_2$) nanostructures with the aid of a post-treatment with non-fluorinated octadecyltrimethoxysilane (ODS) self-assembled monolayers (SAMs) on fluorine-doped tin oxide (FTO) glass to achieve a wide range of wettability, ranging from superhydrophilic to superhydrophobic. The earth-abundant $Ni(OH)_2$ was chosen because its inherent chromogenic property can achieve a high transparency *via* optimal heat treatment. In addition, the stepwise anodic electrodeposition of nanoporous $Ni(OH)_2$ is cost-effective, relatively fast, as well as offering good ease of controlling and reproducing surface morphologies.[23] Here, the nanoporous coating of $Ni(OH)_2$ having exposed hydroxide ligands not only serves as a seed layer to create nanoscale roughness for water penetration but also enhances the surface adsorption of ODS-SAMs for air trapping. Finally, the effectiveness of these achieved functions is demonstrated in the promising applications of two-dimensional (2D) microchannels based on surface-tension confinement.[24] Here, a new method using simple electrochemical attach–detach technique was developed to create the pattern with great wetting contrast between the superhydrophobic coating of nanoporous $Ni(OH)_2$ and the hydrophilic FTO surface.

Experimental

Tunable hydrophilic/superhydrophilic nanoporous films

The experiments were carried out using an anodically electroplated $Ni(OH)_2$ film on FTO glass followed by chemical modification of the ODS-SAMs. A CHI 660E potentiostat/galvanostat was used in the electrochemical process in a standard three-electrode system with a platinum mesh as the counter electrode and a saturated Ag/AgCl as the reference electrode. FTO glass (1 cm × 1.5 cm) having a sheet resistance of 8 Ω $\square^{-1}$ and optical transmittance of 80% was first rinsed with 4% PK-LCG545 (Parker Corp.) and deionized water at 50 °C for 15 min with sonication, respectively. The clean FTO glass was then immersed into a neutral plating solution of 0.13 M sodium acetate, 0.13 M nickel sulfate and 0.1 M sodium sulfate at room temperature.[25] The single-step, two-step and three-step constant current densities were employed for anodic electrodeposition. In the case of single-step deposition, the current density was set to 0.5 mA cm^{-2} for 30 min. The current density profile of two-step deposition started from 0.05 mA cm^{-2} for 30 min and continued on 0.5 mA cm^{-2} for another 30 min. The three-step deposition started from very low current density of 0.005 mA cm^{-2} for 30 min and then jumped to 0.05 mA cm^{-2} for 30 min and continued on 0.5 mA cm^{-2} for the last 30 min. All samples showed similar thickness which was mainly dominated by the final deposition step (0.5 mA cm^{-2} for the 30 min). WCAs were measured using a contact angle goniometer (Sindatek Model 100SB) in five different points on the as-prepared samples. The as-prepared electroplated $Ni(OH)_2$/FTO samples were annealed at 120 °C for 1 h before ODS treatment. After annealing, the color of the $Ni(OH)_2$ film changed from dark to transparent.

Tunable hydrophobic/superhydrophobic nanoporous films after ODS post-treatment

The annealed samples were then immersed into a solution of 3% (v/v) octadecyltrimethoxysilane (ODS) and 0.5% (v/v) butylamine in toluene for 20 min. Subsequently, the samples were annealed at 100 °C for 1 h to form tight hydrogen bonds between the hydroxyl groups of the $Ni(OH)_2$ films and the hydrolyzed trimethoxy groups of ODS. WCAs were measured on ODS/$Ni(OH)_2$/FTO glass using the same procedure.

Electrochemical attach–detach method of 2D microfluidic channel

Referring to Fig. 1(a), a 50 μm-thick chemical-resist sticker (Max Bepop, CM-200E) was used as a mask with an interior

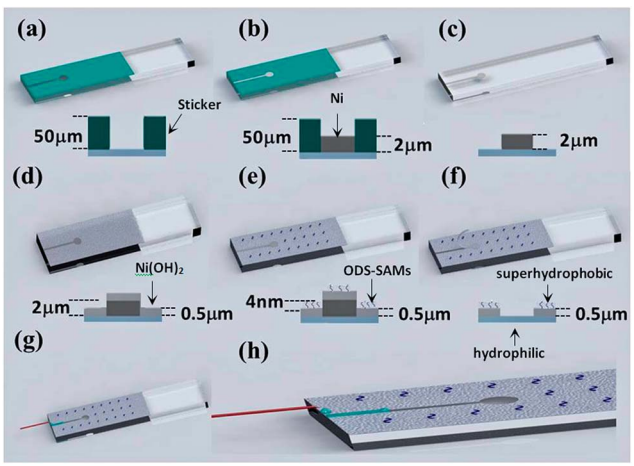

Fig. 1 The process flow for fabrication of a patterned ODS/3-$Ni(OH)_2$ layer on FTO substrate. (a) A patterned, chemical-resist sticker partly attached on FTO glass (the right-hand side of the transparent FTO glass was left for being clipped). (b) Metallic nickel layer was electroplated on the exposed bottle-shaped FTO glass. (c) The sticker was removed and a bottle-shaped nickel mask was achieved. (d) The 3-$Ni(OH)_2$ film was anodically electroplated on the whole surface. (e) ODS modification on the whole surface. (f) Bottle-shaped nickel mask was removed and the superhydrophobic–hydrophilic micropattern was created. (g) The microfluidic drops of green water inks flowed along the hydrophilic domain. (h) Local enlargement of (g).

bottle-shaped microchannel on FTO glass, where the width is 500 μm, the length is 8.4 mm and the diameter of the circle is 2 mm. A 2 μm-thick nickel layer was then electroplated on the exposed bottle-shaped region from a commercial electrolyte (Caswell Inc.) and thereby the bottle-shaped nickel layer was achieved on FTO after detaching the sticker, as seen in Fig. 1(b) and 1(c). Here, nickel was chosen because it can resist the chemicals in the following processes of anodic $Ni(OH)_2$ electroplating and ODS treatment. This intact electroplated nickel layer serves as a mask to protect the underneath hydrophilic FTO surface, and can be simply removed afterwards. Fig. 1(d) and 1(e) show that 500 nm-thick 3-$Ni(OH)_2$ (3-step deposited $Ni(OH)_2$) was anodically electroplated on the whole surface followed by ODS-SAMs modification. Lastly, the patterned nickel layer can be simply detached using ordinary tape due to its weak adhesion on the smooth FTO surface so that the predetermined design of the bottle-shaped microchannel can be obtained,[26] as seen in Fig. 1(f). Fig. 1(g) and 1(h) are the schematic of the 2D microchannel with the superhydrophobic ODS/3-$Ni(OH)_2$ layer and the hydrophilic FTO surface.

Results and discussion

3-D nanosponge-like nickel hydroxide

The single-step, two-step and three-step constant current densities were employed to anodically electrodeposit the nanoporous $Ni(OH)_2$ films on the FTO glass, represented as 1-, 2- and 3-$Ni(OH)_2$/FTO hereafter. Fig. 2(a) shows that bare-FTO is polycrystalline and the deposited 3-$Ni(OH)_2$/FTO exhibited a three-dimensional (3D) nanosponge-like structure (Fig. 2(b)) constructed by the interconnected nanosheets (Fig. 2(c)). The corresponding selected-area electron-diffraction (SAED) pattern in the inset of Fig. 2(c) identified that the polycrystalline α-$Ni(OH)_2$ film was formed after the annealing process (JCPDS card no. 22-0444). Fig. 2(d)–(f) show the top view FE-SEM images of 1-, 2-, and 3-$Ni(OH)_2$/FTO with average pore sizes of 30 nm, 75 nm and 150 nm, respectively. As known, the nucleation rate of electrochemical deposition is correlated to the overpotential and the current density. In general, the higher overpotential and current density lead to the higher nucleation rate. For the anodic electrodeposition of $Ni(OH)_2$ films, the nuclei are initially electrodeposited on active sites on FTO (crystal defects, atomic step, grain edge) and the nucleation model corresponds to the instantaneous mode where the growth of nuclei on active sites occurs in a very short time period. The following ions are preferentially deposited on these nuclei in order to minimize the surface energy and then grow into the nanoporous structures. For 3-$Ni(OH)_2$/FTO, the initial stage of anodic electrodeposition on FTO was at the low current density of 0.005 mA cm^{-2} so that the growth of nuclei only occurred on a small number of active sites, leading to a larger pore size. Accordingly, the small pore size of 1-$Ni(OH)_2$/FTO can be understood by the initial high current density of 0.5 mA cm^{-2}. Therefore, the initial current density of anodic electrodeposition determines the resulting pore sizes of the $Ni(OH)_2$ films (Fig. S1†). Additionally, it was observed that the hierarchical three-step current densities (0.005 mA cm^{-2}, 0.05 mA cm^{-2}, 0.5 mA cm^{-2}) could grow $Ni(OH)_2$ films having a strong adhesion on FTO. Otherwise, if the current density suddenly jumped from 0.005 to 0.5 mA cm^{-2}, the stacking faults increased the film strain and stress, causing the film to peel off spontaneously.

Tunable wettability between superhydrophilic to superhydrophobic

The wettability of bare-FTO and the as-prepared $Ni(OH)_2$/FTO were investigated by measuring the static WCAs using deionized water as a probing liquid. As shown in the black curve of Fig. 3, FTO became hydrophilic and superhydrophilic with the introduction of nanoporous $Ni(OH)_2$ films. As seen, the WCAs were obviously decreased with increasing deposition steps due to the increase of surface roughness from 30.4 nm to 41.4 nm (Fig. S2†). In our case, the water droplet was prone to penetrate completely into the asperities on $Ni(OH)_2$/FTO because the hydroxyl groups enabled the formation of hydrogen bonds between $Ni(OH)_2$ and water molecules. This scheme fits the Wenzel's model which predicts that the intrinsically hydrophilic surface becomes more hydrophilic due to the increase of the solid–liquid interface when increasing the surface roughness.[27] Furthermore, the top and side water penetration into the 3D

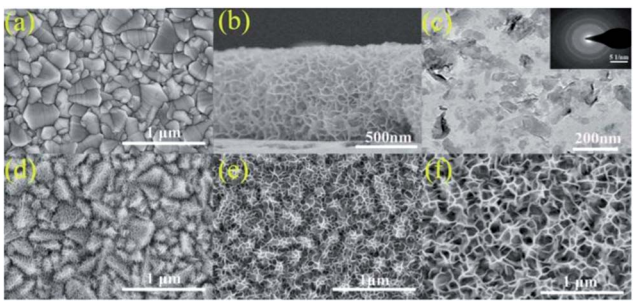

Fig. 2 (a) FE-SEM image of bare-FTO. (b) Cross sectional FE-SEM image and (c) TEM image of 3-$Ni(OH)_2$/FTO. The corresponding SAED pattern is shown in the inset of (c). Top view FE-SEM images of (d) 1-$Ni(OH)_2$/FTO, (e) 2-$Ni(OH)_2$/FTO and (f) 3-$Ni(OH)_2$/FTO.

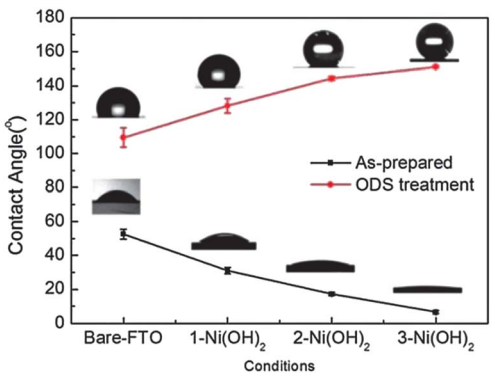

Fig. 3 WCAs of bare-FTO and various $Ni(OH)_2$/FTO (■) as-prepared samples and (●) ODS-modified samples.

nanosponge-like structure of 3-$Ni(OH)_2$/FTO because of the capillary force makes the surface superhydrophilic. Also, the small standard deviation of WCAs for 3-$Ni(OH)_2$/FTO indicates the uniform $Ni(OH)_2$ coating on FTO.

Bare-FTO and annealed $Ni(OH)_2$/FTO were subsequently modified with a 3% solution of ODS in toluene for 20 min in ambient atmosphere and were noted as ODS/FTO and ODS/$Ni(OH)_2$/FTO. As known to the formation of SAMs, the hydrolysable end-groups of ODS react with the hydroxyl groups presented on the substrate surface to form silanol (Si–OH) groups and then the Si–OH groups condense with each other to form a polysiloxane (Si–O–Si) network.[28] Here, the nanoporous $Ni(OH)_2$ plays an important role in providing terminated hydroxyl groups and large surface area, which can significantly promote the surface coverage of the ODS-SAMs (Fig. S3†). It is also worthy to note that the ODS-SAMs modification has little effect on the change of roughness and morphology (Fig. S4†). As seen in the red curve of Fig. 3, all the sample surfaces were altered to a hydrophobic property because the surface energy was reduced by the exposed long outer hydrocarbon chains of the ODS-SAMs and the WCAs on the ODS/$Ni(OH)_2$/FTO sampels increased with the increasing number of deposition steps. In this case, when ODS/$Ni(OH)_2$/FTO was in contact with the water droplet, the non-polar long hydrocarbon chains of the ODS-SAMs preferred to contact with air and the nanoporous structures could easily trap air, forming a composite surface comprising an ODS–water interface (solid–liquid) and an air–water interface (air–liquid). Moreover, the larger the pore size, the more the air was trapped, leading to an increased hydrophobicity when changing the deposition conditions from single-step to three-step. As known, another well-known Cassie–Baxter's model is more comprehensive when dealing with a heterogeneous surface, which predicts that the hydrophobicity increases with increasing the surface roughness and the fraction of the air pockets.[29] Calculated from SEM images (Fig. 2), the air fractions increase from 0.41 to 0.75 when changing the deposition conditions from single-step to three-step due to the increase of the pore sizes. Fig. S5† shows that the increased trend of hydrophobicity corresponds to Cassie–Baxter's model rather than Wenzel's model. Consequently, ODS/3-$Ni(OH)_2$/FTO achieves superhydrophobicity with WCAs of 151° and the sliding angle is around 5° (Fig. S6†).

Superhydrophobicity and non-degraded transparency

The excellent water-repellency can be seen in Fig. 4(a), showing a completely non-wetting behavior between ODS/3-$Ni(OH)_2$/FTO and the water droplet over several tens of cycles (Video S2†). Based on the shape deformation and considering the vertical force balance, the adhesion force (f) between the water droplet and ODS/3-$Ni(OH)_2$/FTO could be quantitatively calculated using eqn (1),[30]

$$f = \pi R_x \gamma (1 - R_x/R_y) - \rho V g \quad (1)$$

where γ is the surface tension of water, and R_x and R_y are the principal radii of curvature. The last term represents the gravitational force acting on the lower part of the water droplet, where ρ and V are the density and volume of the lower part of the water droplet, and g is the gravitational acceleration.

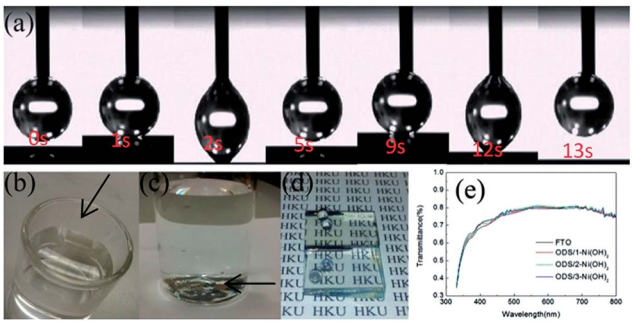

Fig. 4 Photographs of (a) water-repellent property of ODS/3-$Ni(OH)_2$/FTO during cyclic measurement of WCAs, (b) ODS/3-$Ni(OH)_2$/FTO floating on water, (c) bare-FTO sinking to the bottom of water, (d) the pearl-shaped water droplets on the transparent ODS/3-$Ni(OH)_2$/FTO and (e) UV-vis spectra of bare-FTO and ODS/$Ni(OH)_2$/FTO of the three different deposition conditions.

The corresponding adhesion forces of attachment (1 s) and before detachment (2 s) are 8.11 μN and 53 μN. The latter value is between two well-known superhydrophobic plants: lotus leaf (8–18 μN) and *Euphorbia myrsinites* (30–58 μN).[31] Jin *et al.* also reported that adhesion force over 60 μN would exhibit a highly adhesive superhydrophobic surface even if the substrate was tilted to 180° based on a highly-sensitive microelectromechanical balance system.[32] In fact, superhydrophobic phenomena are ubiquitous in nature and another well-known example is the water strider (family Gerridae) whose legs are able to support itself statically on top of the water surface.[33] Interestingly, the identical phenomenon was reproduced when ODS/3-$Ni(OH)_2$/FTO was gently placed on top of the water surface; conversely, bare-FTO directly sank to the bottom of the water container, as shown in Fig. 4(b) and 4(c), respectively. Fig. 4(d) demonstrates that the ODS/3-$Ni(OH)_2$/FTO is superhydrophobic and optically transparent with the pearl-shaped water droplets and the HKU characters underneath can clearly be seen. As shown in Fig. 4(e), UV-visible spectra show that the transmittance of the ODS/$Ni(OH)_2$/FTO was slightly enhanced in the ultraviolet (UV) range and maintainable in the visible range compared with bare-FTO. The reason might be that the nanoporous $Ni(OH)_2$ coating is a transparent material with sub-wavelength pore sizes so that reflectance and the Mie scattering effect are effectively reduced.[34]

2D transparent microfluidic channels

As mentioned earlier, a wide range of tunable wettability with highly optical transparency is applicable in various applications. 2D transparent microchannels were chosen here to demonstrate this potential using superhydrophobic ODS/3-$Ni(OH)_2$/FTO as the substrate. Compared with conventional 3D microchannels, open-air 2D microchannels facilitate the inlet access and observation for the versatile behaviors of microfluidic drops, such as transporting, mixing and reactions. In

this work, we also presented a new patterning technique using a simple electrochemical attach–detach method to fabricate the 2D microchannel, which is more cost-effective compared with conventional photolithography or microcontact stamp-printing.

Fig. 5(a) and 5(b) show the photographs of the 2D microchannel filled with green water inks from the top and side views. In principle, the propagation of microfluids in the 2D microchannels could be driven by capillary force, gravitational force, surface vibration and surface tension gradient.[35] In our case, the superhydrophobic region (ODS/3-Ni(OH)$_2$/FTO) serves as a virtual wall while the hydrophilic region (FTO) generates the capillary force. The resulting wetting contrast leads microfluids to move along the defined hydrophilic path. Lam *et al.* reported that the movement of microfluids in the 2D microchannel is correlated to the microchannel geometry, the surface tension of the liquid and the WCAs of the hydrophilic path.[24] When taking the latter two parameters as constants, the flow speed is dominated by the microchannel geometry. In general, a large height difference retards the motion of microfluidic drops due to the weak capillary force. Fig. 5(c) and 5(d) are the top view and cross-sectional FE-SEM images of the 2D microchannel, showing the width of 500 μm, the diameter of 2 mm and the height difference of 500 nm between the hydrophilic FTO surface and the superhydrophobic ODS/3-Ni(OH)$_2$ layer. As noted, most of the reported height difference in the 2D microchannels was in the microscale which was much thicker than ours. The measured flow speed of the deionized water droplets transporting in our microchannel was about 5 mm s^{-1}. Compared with the 2D microchannel fabricated on the microporous polymer film with the height difference of 40 μm, the same flow speed can only be reached by using a low-viscosity liquid of mixed acetonitrile and deionized water.[36] As clearly seen in ESI Video S3†, the green water drops are propagated quickly along the 2D microchannel without external propelling forces as if a virtual wall was surrounding to guide and confine the microfluidic drops.

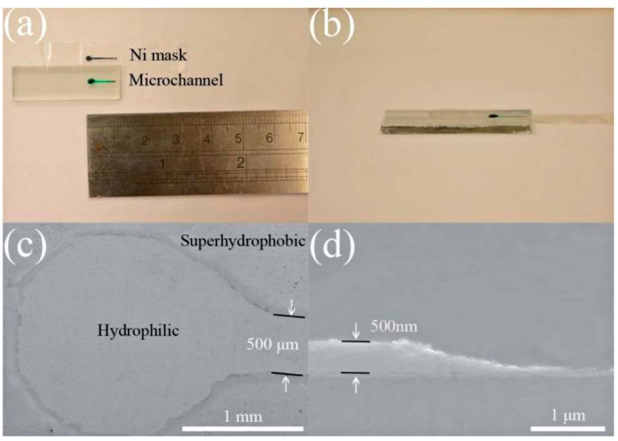

Fig. 5 The photographs of the 2D transparent microchannel showing (a) top and (b) side views. The FE-SEM images of the 2D microchannel showing (c) top view and (d) cross-sectional view.

Conclusions

In summary, we present a facile approach to achieve a widely tunable wettability ranging from superhydrophilicity to superhydrophobicity by the stepwise anodic electrodeposition of 3D nanosponge-like Ni(OH)$_2$ on FTO with the aid of post-treatment with ODS-SAMs. The hydroxide ligands of the nanoporous Ni(OH)$_2$ films not only serve as the seed-layer to create nanoscale roughness for water penetration but also enhance the surface coverage of the ODS-SAMs for air trapping. The high optical transparency is maintainable and the superhydrophobic surface is achieved by this new method and will be of great potential for various optical applications. We demonstrate this potential on the 2D microchannels with a flow speed of 5 mm s^{-1} using the wetting contrast between the superhydrophobic ODS/3-Ni(OH)$_2$ layer and hydrophilic FTO surface. In addition, we developed a simple and cost-effective patterning technique using the electrochemical attach–detach method to fabricate the 2D microchannel. The findings are expected to stimulate fundamental research interest and practical applications for using the distinctive wettability of nanoporous metal hydroxides fabricated by electrochemical processes.

Acknowledgements

The authors thank Dr. Wallace C. H. Choy and Mr. Lixh Li for the assistance of transmittance measurement and Dr. Cheong-Wei Chong and Dr. Chien-Cheng Li for the assistance of AFM measurement. This work was supported by the General Research Fund from Research Grants Council of Hong Kong Special Administrative Region, China, under Award Number: HKU 719512E.

Notes and references

1 K. Liu, X. Yao and L. Jiang, *Chem. Soc. Rev.*, 2010, **39**, 3240–3255.
2 B. Bhushan and Y. C. Jung, *Prog. Mater. Sci.*, 2011, **56**, 1–108.
3 L. Mishchenko, B. Hatton, V. Bahadur, J. A. Taylor, T. Krupenkin and J. Aizenberg, *ACS Nano*, 2010, **4**, 7699–7707.
4 M. Nosonovsky and B. Bhushan, *Curr. Opin. Colloid Interface Sci.*, 2009, **14**, 270–280.
5 W. Jiang, G. Wang, Y. He, X. Wang, Y. An, Y. Song and L. Jiang, *Chem. Commun.*, 2005, 3550–3552.
6 X. Zhang, F. Shi, J. Niu, Y. G. Jiang and Z. Q. Wang, *J. Mater. Chem.*, 2008, **18**, 621–633.
7 V. A. Lifton and S. Simon, *J. Porous Mater.*, 2011, **18**, 535–544.
8 S. T. Wang, L. Feng, H. Liu, T. L. Sun, X. Zhang, L. Jiang and D. B. Zhu, *ChemPhysChem*, 2005, **6**, 1475–1478.
9 Y. Y. Yan, N. Gao and W. Barthlott, *Adv. Colloid Interface Sci.*, 2011, **169**, 80–105.
10 A. I. Aria and M. Gharib, *Langmuir*, 2011, **27**, 9005–9011.
11 A. Kumar, N. L. Abbott, E. Kim, H. A. Biebuyck and G. M. Whitesides, *Acc. Chem. Res.*, 1995, **28**, 219–226.
12 N. Verplanck, Y. Coffinier, V. Thomy and R. Boukherroub, *Nanoscale Res. Lett.*, 2007, **2**, 577–596.

13 Y. F. Li, J. H. Zhang, S. J. Zhu, H. P. Dong, Z. H. Wang, Z. Q. Sun, J. R. Guo and B. Yang, *J. Mater. Chem.*, 2009, **19**, 1806–1810.
14 G. Birarda, G. Grenci, L. Businaro, B. Marmiroli, S. Pacor and L. Vaccari, *Microelectron. Eng.*, 2010, **87**, 806–809.
15 K. H. Tantawi, W. Gaillard, J. Helton, E. Waddell, S. Mirov, V. Fedorov and J. D. Williams, in *Southeastcon, 2012 Proceedings of IEEE*, 2012, pp. 1–4.
16 E. Ueda and P. A. Levkin, *Adv. Mater.*, 2013, **25**, 1234–1247.
17 W. Shen, M. Li, C. Ye, L. Jiang and Y. Song, *Lab Chip*, 2012, **12**, 3089–3095.
18 H. M. Shang, Y. Wang, S. J. Limmer, T. P. Chou, K. Takahashi and G. Z. Cao, *Thin Solid Films*, 2005, **472**, 37–43.
19 S. Jindasuwan, O. Nimittrakoolchai, P. Sujaridworakun, S. Jinawath and S. Supothina, *Thin Solid Films*, 2009, **517**, 5001–5005.
20 X. Deng, L. Mammen, Y. F. Zhao, P. Lellig, K. Mullen, C. Li, H. J. Butt and D. Vollmer, *Adv. Mater.*, 2011, **23**, 2962–2965.
21 J. T. Han, S. Y. Kim, J. S. Woo and G. W. Lee, *Adv. Mater.*, 2008, **20**, 3724–3727.
22 G. Z. Shen, B. Liang, X. F. Wang, H. T. Huang, D. Chen and Z. L. Wang, *ACS Nano*, 2011, **5**, 6148–6155.
23 T. Darmanin, E. T. de Givenchy, S. Amigoni and F. Guittard, *Adv. Mater.*, 2013, **25**, 1378–1394.
24 P. Lam, K. J. Wynne and G. E. Wnek, *Langmuir*, 2002, **18**, 948–951.
25 D. Tench and L. F. Warren, *J. Electrochem. Soc.*, 1983, **130**, 869–872.
26 R. Zheng, J. Gao, J. Wang, S.-P. Feng, H. Ohtani, J. Wang and G. Chen, *Nano Lett.*, 2011, **12**, 188–192.
27 R. N. Wenzel, *J. Phys. Colloid Chem.*, 1949, **53**, 1466–1467.
28 A. Ulman, *Chem. Rev.*, 1996, **96**, 1533–1554.
29 A. B. D. Cassie and S. Baxter, *Trans. Faraday Soc.*, 1944, **40**, 546–551.
30 X.-D. Zhao, H.-M. Fan, J. Luo, J. Ding, X.-Y. Liu, B.-S. Zou and Y.-P. Feng, *Adv. Funct. Mater.*, 2011, **21**, 184–190.
31 H. J. Ensikat, P. Ditsche-Kuru, C. Neinhuis and W. Barthlott, *Beilstein J. Nanotechnol.*, 2011, **2**, 152–161.
32 M. Jin, X. Feng, L. Feng, T. Sun, J. Zhai, T. Li and L. Jiang, *Adv. Mater.*, 2005, **17**, 1977–1981.
33 X. Gao and L. Jiang, *Nature*, 2004, **432**, 36.
34 S. Chattopadhyay, Y. F. Huang, Y. J. Jen, A. Ganguly, K. H. Chen and L. C. Chen, *Mater. Sci. Eng., R*, 2010, **69**, 1–35.
35 I. You, N. Yun and H. Lee, *ChemPhysChem*, 2013, **14**, 471–481.
36 D. Zahner, J. Abagat, F. Svec, J. M. J. Frechet and P. A. Levkin, *Adv. Mater.*, 2011, **23**, 3030–3034.

